ORIGINAL PAPER

Microstructure and properties of 1100 MPa grade low-carbon hot-rolled steel by laser welding

Chen Dong[1,2] · Ai-min Zhao[1,2] · Xi-tao Wang[1] · Qi-hang Pang[2] · Hui-bin Wu[1,2]

Abstract

The microstructure and mechanical properties of the butt joint of 1100 MPa grade hot-rolled low-carbon steel by laser welding were investigated by scanning electron microscopy, micro-hardness and tensile tests. The yield strength and tensile strength of the laser welded joint reached 100.2 and 99.5% of the base material (BM), respectively. However, the elongation of the welded joint only reached about 60% of BM. The lowest and highest hardness areas both existed in the incomplete recrystallization zone. The width of the softened area of the welded joint is about 240–260 μm. The element distribution has no obvious change for C, Cr, Si, Mn, Ti, etc.

Keywords Hot-rolled steel · Laser welding · Microstructure · Mechanical property · Element distribution

1 Introduction

High-strength low-alloy (HSLA) steels are commonly used in mining machinery, construction cranes, transport heavy machinery, automotive, building, bridges, etc. In order to reduce the weight of vehicle, crane arms, and constructional components, it needs to continuously improve the strength and toughness [1–3]. With a long history of development, the yield strength of hot-rolled HSLA steel had reached 520–850 MPa, while the 1100 MPa grade one was rarely reported.

The laser welding technology with high energy density, high welding speed, narrow heat affected zone, low distortion and large depth to width ratio is an extremely effective joining method. The utilization of laser welding not only enhances the performance of connected materials, but also improves their high-quality assurance [4–8]. Many researchers [9–12] analyzed the microstructures and properties of

DP1000 steels by laser welding. They found that serious softening arose in the heat affected zone (HAZ), most in the tempering zone and incomplete crystalline zone of HAZ. Guo et al. [13] studied the S960 steel plates and found that the tensile properties of the laser welded joint matched those obtained for the base material (BM). However, the DP1000 steels are cold rolled and the S960 steels are quenched in the final treatment.

In this work, a laboratory-made hot-rolled low-carbon steel with yield strength of 1100 MPa and excellent elongation was successfully processed. And the microstructures and properties of the steel by laser welding were studied. The influence of the laser welding on the fracture morphology, the forming mechanism of the softened zone in HAZ, and the elements distribution of the welded joint were also investigated.

2 Experiment procedure

The experimental steels were smelted in a vacuum furnace with a maximum melting capacity of 25 kg, and then cast and forged into small cubes of 60 mm × 70 mm × 80 mm. The chemical compositions (wt%) are C 0.10, Si 0.24, Mn 0.99, Ni 0.32, Cr 1.09, Cu 0.25, Al 0.03, Mo 0.21, (Nb + Ti + V) 0.1, B 0.002, and Fe balance. The cubes were heated to 1200 °C for 2 h and rolled into 4.5-mm-thick steel plates with a ϕ450 mm trial rolling mill. The finish

✉ Ai-min Zhao
  zhaoaimin@ustb.edu.cn

✉ Xi-tao Wang
  xtwang@ustb.edu.cn

1   Collaborative Innovation Center of Steel Technology, University of Science and Technology Beijing, Beijing 100083, China

2   Engineering Research Institute, University of Science and Technology Beijing, Beijing 100083, China

rolling temperature was set as 850 °C, and then the plates were water cooled to 350 °C and held in the heat preservation furnace for 1.5 h. Finally, the plates were air cooled to room temperature. The microstructures of the base material are lath bainite and lots of dispersed carbides as shown in Fig. 1a, b.

The butt welding was performed using a Slab DC 035 CO_2 laser with a power output of 3 kW and a welding speed of 2 m min^{-1}. Argon gas was used to protect the melt pool from oxidization. The samples of the welded joint were polished and etched with 4 vol.% nital for microstructure observation. The microstructures were analyzed with the Quanta 450 scanning electron microscopy (SEM). The tensile tests were analyzed with the CMT-4105 tensile machine at a constant strain rate of 1 mm min^{-1}. The gauge length of the extensometer used was 50 mm. The HVS-1000 micro-hardness tester was used to measure the hardness.

3 Results and discussion

3.1 Tensile properties

The tensile properties of the base metal and welded joint were tested several times, and the results are shown in Fig. 2. It shows that the strength of the high-strength steels after laser welding is almost the same high as the base metal; however, the elongation of the welding joint has a significant decline from about 10 to 6%. Figure 3a shows the typical pure shear fracture of the tensile tests of the laser welded joint. The plane of the fracture is formed at about 45° with the tensile axis, and the surface of the fracture is relatively bright. The location of the fracture is near the welding seam as shown in Fig. 3a, which illustrates the decrease of the properties is due to the variations of the microstructures of the joint after laser welding. Combining the analysis of
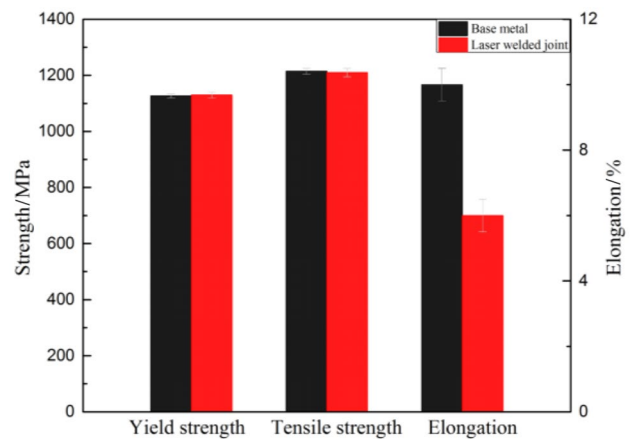

Fig. 2 Tensile properties of base metal and laser welded joint

the hardness distribution of the welding joint as shown in Fig. 4b, it can be determined that the softening zone (about 320 HV) of HAZ was the initiative place of cracks during the tensile tests. Because the length of the softening zone is quite short (about 0.25 mm, see below) and the length of the welding seam (2.0–2.5 mm) is about half of the thickness of the plate (about 4.5 mm), the fracture crossed the fusion zone (about 380 HV) and base metal (about 360 HV). By the combined effect of each zones, the yield strength and tensile strength of the welding joint reached 100.2 and 99.5% of BM. Because the microstructure of the fusion zone is martensite, the elongation of the welding joint fell 4%.

Figure 3b–d shows that the morphology of the fracture can be divided into 3 classes: first class, the small equi-axed dimples which are deep and with a diameter of about 0.5–2.5 µm (measured by Image-Pro Plus, the same below); second class, the coarse equiaxed dimples which are shallow and with a diameter of about 3–6 µm; third class, the big elongated dimples (like a worm). It has a deep dimple
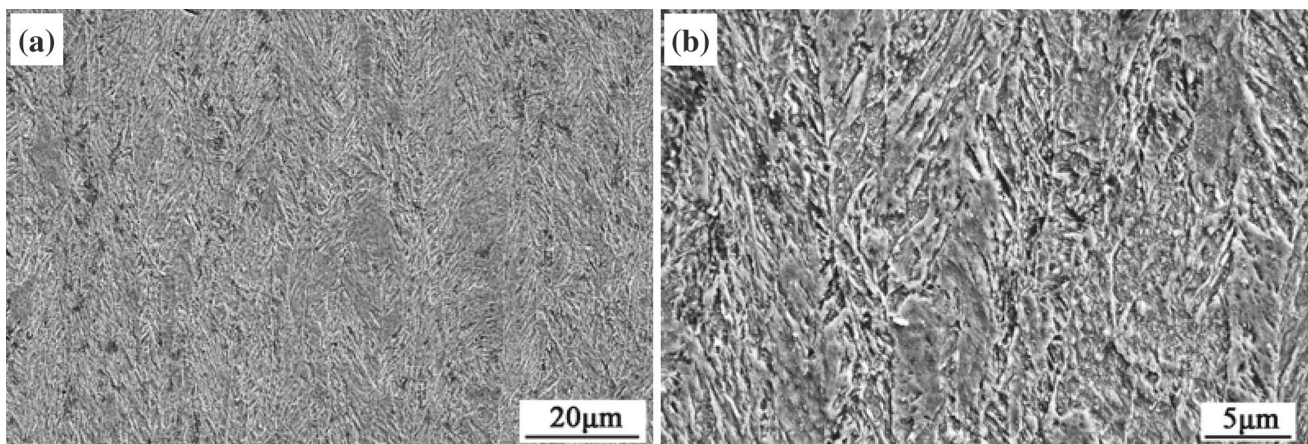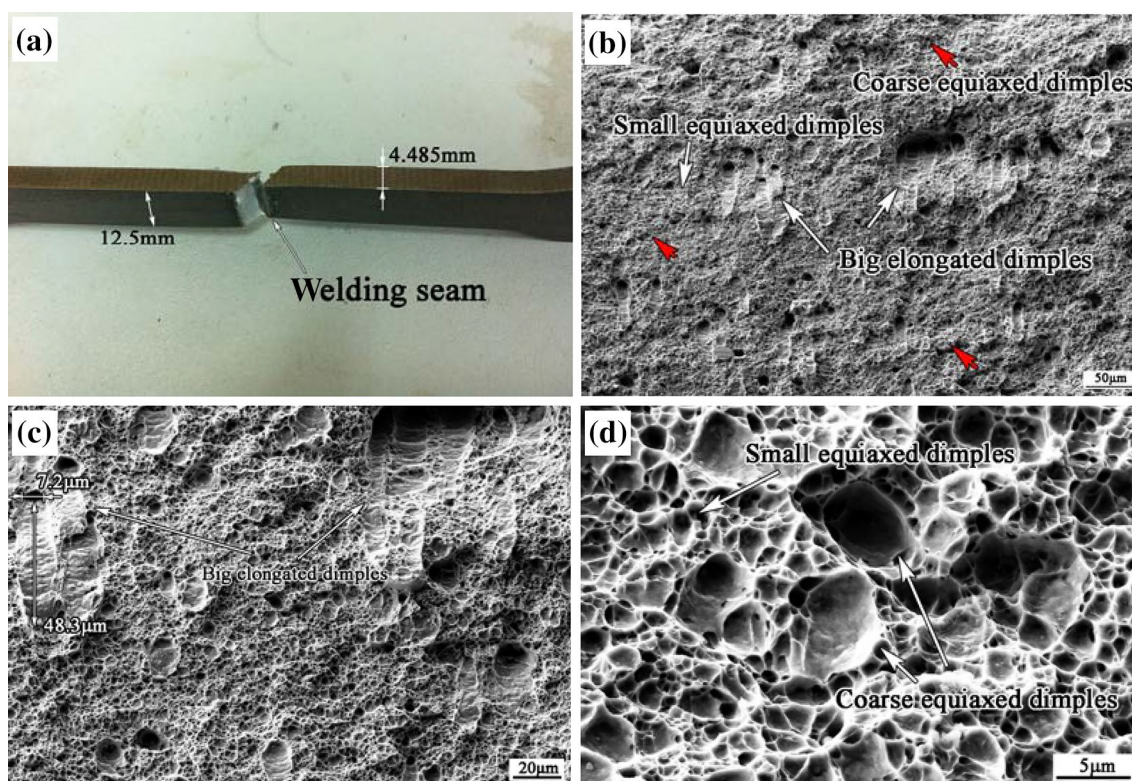

Fig. 1 Low-magnification (**a**) and high-magnification (**b**) SEM images of base metal

Fig. 3 Typical pure shear fracture of tensile tests of laser welded joint (**a**) and macroscopic view of tensile fracture (**b**), big elongated dimples of tensile fracture (**c**) and coarse equiaxed dimples of tensile fracture (**d**)

(like a head with a diameter of about 6–15 µm) and a slip separation (like a worm body with a width bigger than its "head" and a much long length of about 10–60 µm). The distribution directions of the big elongated dimples are the same and parallel to the direction of the shear stress of the tensile tests. Some of the big elongated dimples appear side by side as shown in Fig. 3b.

3.2 Microstructures and micro-hardness

Figure 4a shows the macroscopic image of the laser welded joint. As usual, the welding joint can be divided into three regions: fusion zone (FZ), heat affected zone and base metal zone (BMZ). The HAZ can be subdivided into three regions: tempering zone (TZ), incomplete recrystallization zone (IRZ) and recrystallization zone (RZ). The row of diamond points at the lower side of the image is the indentations of the Vicker's hardness tester (load = 2.94 N). Figure 4b shows the micro-hardness distribution of the welding joint. Figure 4c, d is the local magnifications of Fig. 4a. As shown in Fig. 4c, the sizes of the indentations were measured and written in nearby in the form of (transverse length × longitudinal length, µm). According to the analysis of the indentations of the hardness tests, the boundary between BMZ and HAZ can be accurately determined and the width of

TZ of the welded joint is about 240–260 µm. And the width of IRZ is about 100 µm. Figure 4d shows the details of the fusion line of the welding joint, which can determine that the width of RZ is about 260 µm, and the width of FZ is about 750–1000 µm as shown in Fig. 4a.

As shown in Fig. 4a–c, the hardness of TZ is lower than that of BMZ. Figure 5a, b illustrates the microstructures of TZ. Comparing to the morphology of BMZ as shown in Fig. 1, the lath bainite became blur, the number of dispersed carbides was decreased, and the ferritic major axis began to twist, which are due to the fact that the temperature of TZ during the laser welding is about 150 °C to A_{c1}. As the temperature rises to 150–350 °C, the carbon atoms can diffuse by long range, and the iron atoms can diffuse effectively at the temperature above 500 °C [14, 15]. During the welding, the lath bainite of TZ would gradually transform to a more stable state, i.e., ferrite and cementite. However, the time of the tempering was not long enough and the structures were formed as Fig. 5a, b; the short strip boundaries and the small dispersed carbides of lath bainite gradually disappeared with decreasing strength and hardness.

The hardness of the part close to TZ side of IRZ is the lowest (about 320 HV) of all the places of the visual field as shown in Fig. 4a, b; however, the part close to RZ side of IRZ is the hardest (about 400 HV). Figure 6a shows the
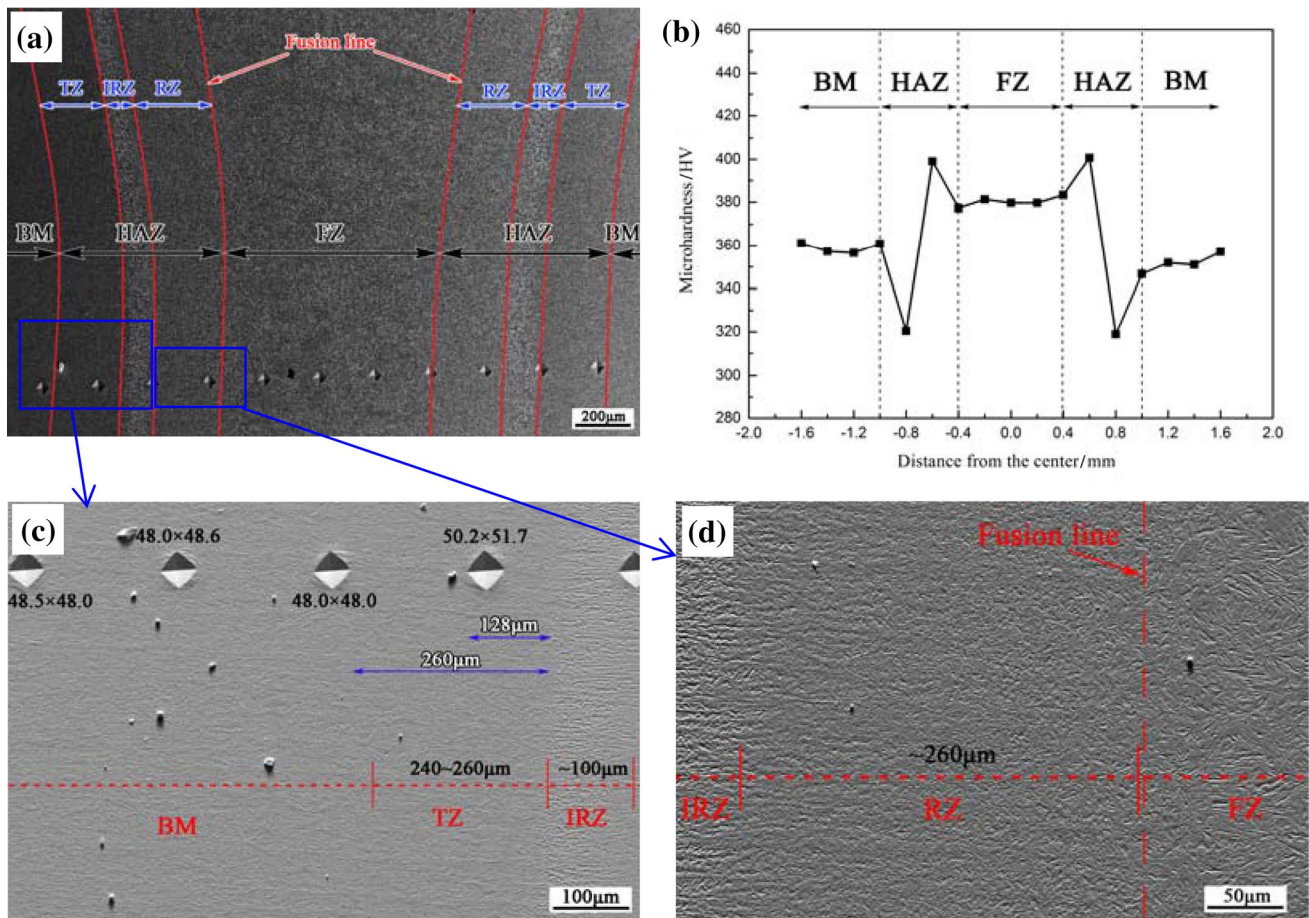
Fig. 4 Macroscopic image of laser welded joint (**a**), micro-hardness distribution (**b**), details of HAZ (**c**), and details of the fusion line (**d**)
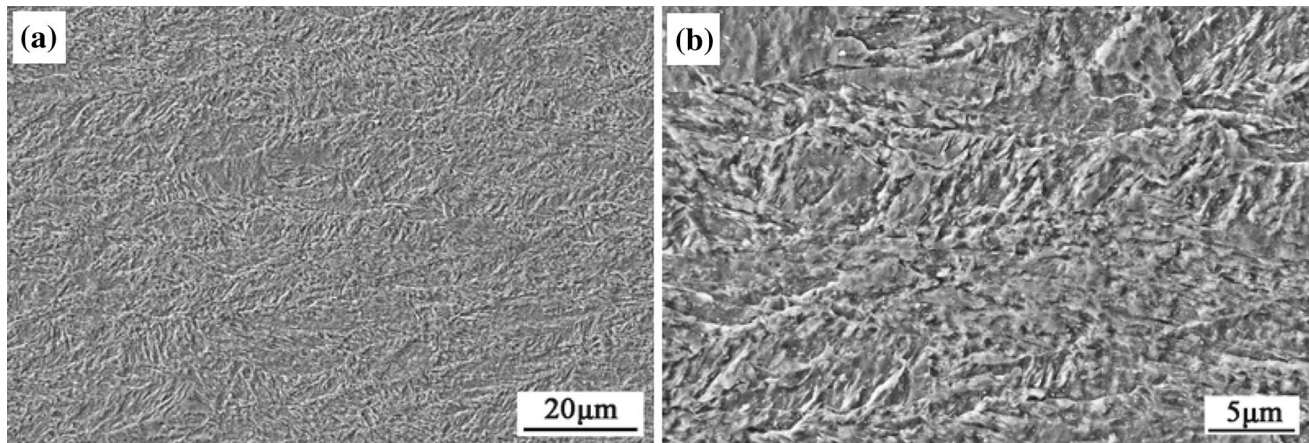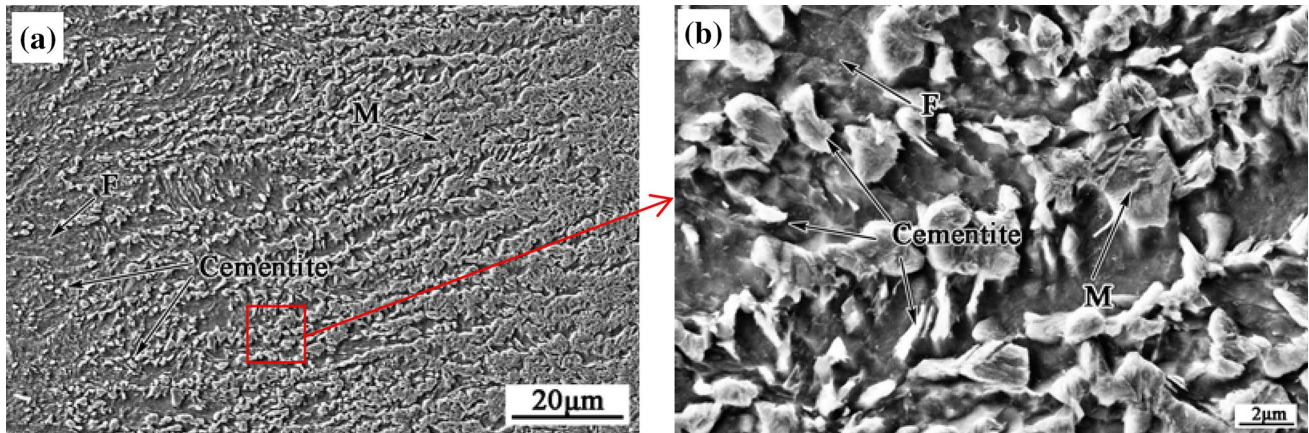

Fig. 5 Low-magnification (**a**) and high-magnification (**b**) SEM images of tempering zone

microstructure of IRZ, and it can be significantly found that the lath bainite transformed into the ferrite and coarse cementite in the left side of the image, and the martensite was formed in the right side. Figure 6b is the local magnification of the middle side of Fig. 6a, which shows the

transitional region of these two extremes. As shown in Fig. 6b, a mix structure of ferrite, cementite and martensite was formed together, reasons of which are that during the welding, the temperature of IRZ rises to A_{c1}–A_{c3}, meaning that a part of the lath bainite was transformed into austenite
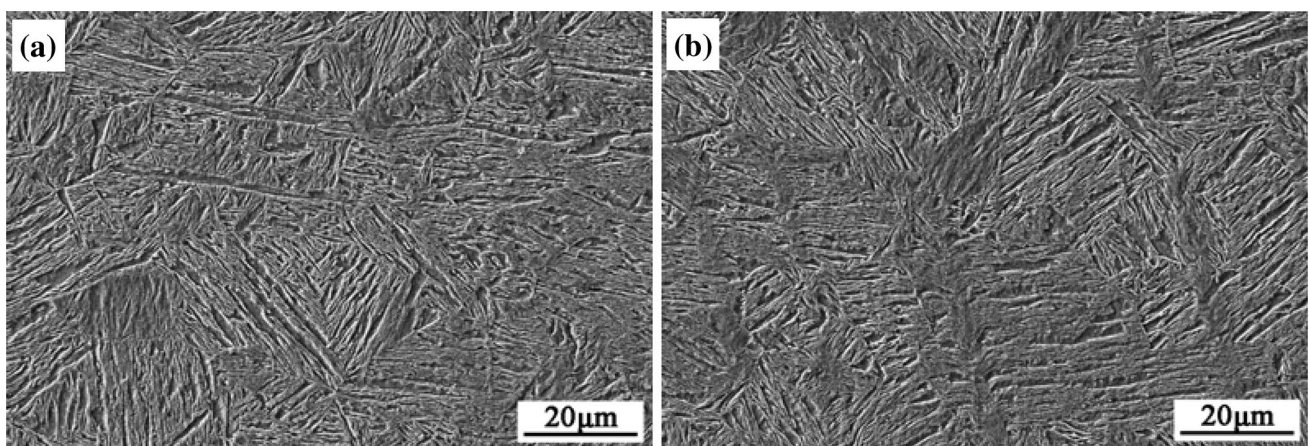
Fig. 6 Low-magnification (**a**) and high-magnification (**b**) SEM image of incomplete recrystallization zone
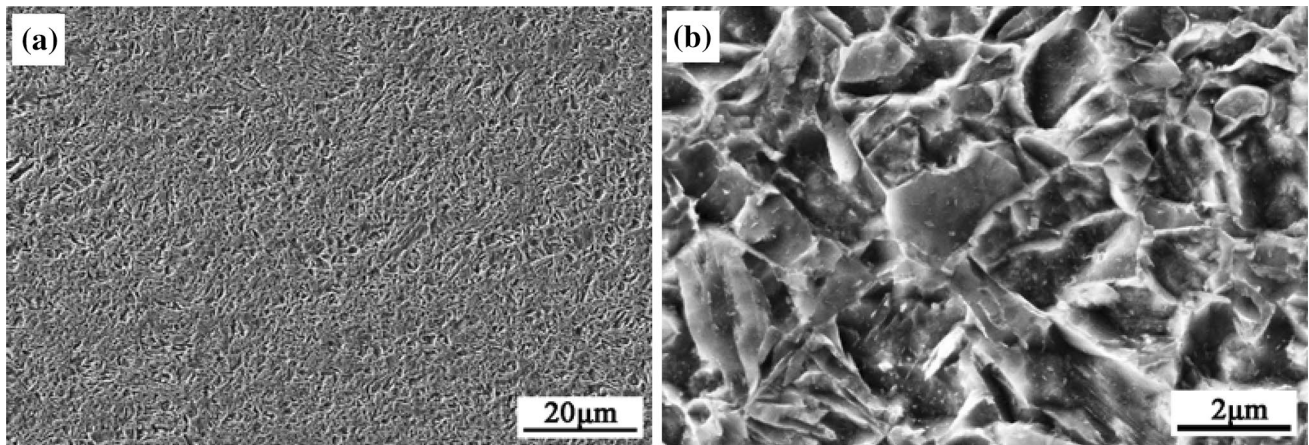
Fig. 7 Low-magnification (**a**) and high-magnification (**b**) SEM images of recrystallization zone

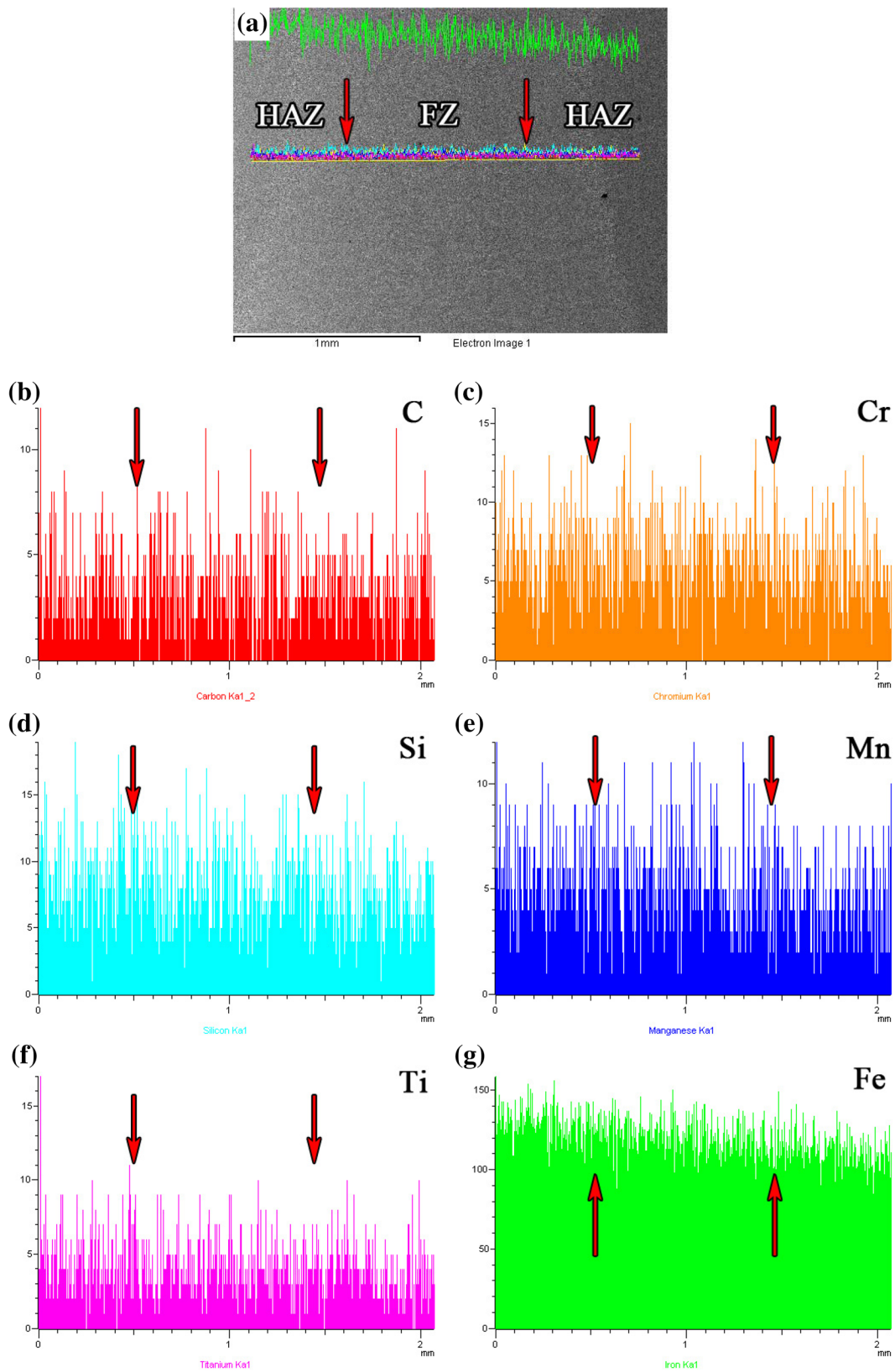**Fig. 8** SEM image of fusion zone close to fusion line (**a**) and at center (**b**)

Fig. 9 Line scan of welded joint by EDS

and then transformed into martensite in the followed cooling. The closer to the fusion zone direction, the more martensite formed. Meanwhile, the formed martensites were distributed in parallel stripped shape for the reason that the austenite nucleated in the boundaries of the lath bainite which were distributed in parallel, as shown in Fig. 1a, b. The forming of lots of ferrite and the coarsening of cementite close to TZ side of IRZ greatly decreased the strength of the material, and the newly formed fine equiaxed martensite close to RZ side of IRZ greatly increased the strength of the metal. The great changes of the strength and hardness in a short region make the property of IRZ unstable. During the uniaxial tensile tests, the crack initiation was around IRZ as shown in Fig. 3a.

Figure 7a, b shows the microstructures of RZ, and the temperature of this area rises to A_{c3}-melting point during the welding. It can be found that the microstructures of RZ are all equiaxed martensite, and the average grain size is about 2–3 μm.

Figure 8a, b shows the microstructures of FZ, and the temperature of this area rises to over melting point during the welding. It shows that the microstructures of FZ are nearly the same: the very coarse equiaxed and columnar tempered martensite. The difference is the change of average grain size from 15–25 μm (edge side, as shown in Fig. 8a) to 25–45 μm (center side, as shown in Fig. 8b). As shown in Fig. 4b, the hardness values of FZ are nearly 380 HV which are lower than those of RZ (about 380–400 HV).

3.3 Element distribution analysis

Figure 9 shows the line scan by EDS of the welded joint. In order to observe the change rules of each element by the effect of laser welding, the red arrows were positioned at the boundary between HAZ and FZ on the left and right as shown in Fig. 9a. It can be seen that the element distribution shows no obvious change for C, Cr, Si, Mn, Ti, etc., which illustrates that the laser welding process is quick and efficient.

4 Conclusions

1. The yield strength and tensile strength of the laser welded joint reached 100.2 and 99.5% of BM, respectively. However, the elongation of the welded joint only

reached about 60% of BM. The reasons are that the main forming of martensite after laser welding strengthened the welded joint and decreased its plasticity significantly.
2. The width of TZ, IRZ, and RZ of the welded joint is about 240–260, ~ 100 and ~ 250 μm, respectively. The lowest hardness (~ 320 HV) area of the laser welded joint is at the part close to TZ side of IRZ, and the highest one (~ 400 HV) is at the part close to RZ side of IRZ.
3. The element distribution has no obvious change for C, Cr, Si, Mn, Ti, etc.

References

[1] H. Xie, L. Du, J. Hu, R.D.K. Misra, Mater. Sci. Eng. A 612 (2014) 123–130.
[2] L.L. Ma, Y.H. Wei, L.F. Hou, J. Iron Steel Res. Int. 23 (2016) 677–684.
[3] Y.J. Qian, W. Yu, H.B. Wu, J. Univ. Sci. Technol. Beijing 5 (2010) 599–604.
[4] W. Meng, Z. Li, J. Huang, Y. Wu, S. Katayama, J. Mater. Eng. Perform. 23 (2014) 538–544.
[5] M. Ghosh, K. Kumar, R.S. Mishra, Scripta Mater. 63 (2010) 851–854.
[6] N. Farabi, D.L. Chen, Y. Zhou, J. Alloy. Compd. 509 (2011) 982–989.
[7] N. Farabi, D.L. Chen, J. Li, Y. Zhou, S.J. Dong, Mater. Sci. Eng. A 527 (2010) 1215–1222.
[8] Q. Jia, W. Guo, W.D. Li, Mater. Sci. Eng. A 680 (2017) 378–387.
[9] J.F. Wang, L.J. Yang, M.S. Sun, T. Liu, H. Li, Mater. Des. 90 (2016) 642–649.
[10] J.F. Wang, L.J. Wang, L.J. Yang, K. Li, X.Y. Li, T. Liu, L.P. Wang, Chinese J. Lasers 41 (2014) No. 9, 0903003.
[11] Y.Z. Zhua, D.M. Liang, J.C. Li, J.P. Xu, Z.L. Xue, Mater. Sci. Eng. A 528 (2011) 8365–8373.
[12] B.S. Xie, Q.W. Cai, W. Yu, J.M. Cao, R. Li, Trans. Mater. Heat Treat. 35 (2014) No. 5, 123–130.
[13] W. Guo, D. Crowther, J.A. Francis, A.Thompson, Z. Liu, L. Li, Mater. Des. 85 (2015) 534–548.
[14] Z.Q. Cui, Y.C. Tan, Metallography & Heat Treatment, China Machine Press, Beijing, 2007.
[15] Q.L. Yong, Secondary Phases in Steels, Metallurgical Industry Press, Beijing, 2006.